Journal of Alloys and Compounds xxx (xxxx) xxx-xxx

Contents lists available at ScienceDirect

Journal of Alloys and Compounds

journal homepage: www.elsevier.com

Rational design of CoNi@C-BTC/rGO nanocomposite coated with PEDOT polymer towards enhancing the microwave absorption in X-band frequency

Yan Cao [a], Abdeliazim Mustafa Mohamed [b], Mehdi Abdollahzadeh [c], Isabelle Huynen [d, *]

[a] School of Mechatronic Engineering, Xi'an Technological University, Xi'an 710021, China
[b] Department of Civil Engineering, College of Engineering, Prince Sattam bin Abdulaziz University, Alkharj 11942, Saudi Arabia
[c] Department of Chemistry, University of Mazandaran, Babolsar, Iran
[d] ICTEAM Institute, ELEN Division, Place du Levant 3, Louvain-la-Neuve B-1348, Belgium

ARTICLE INFO

Article history:
Received 22 September 2020
Received in revised form 19 November 2020
Accepted 14 December 2020
Available online xxx

Keywords:
Graphene
Cobalt nickel-BTC
Solvothermal method
Pyrolysis
Electromagnetic properties
Microwave absorption

ABSTRACT

The present study focusses on the design of microwave absorbers based on CoNi-BTC (CN) mixed with reduced graphene oxide and covered by PDOT to form P@CN/G nanocomposites. They were successfully synthesized via solvothermal method followed by pyrolysis and then characterized with XRD, XPS, VSM and FESEM. CN nanoparticles have an approximately uniform spheroidal monodispersed morphology with 300–400 nm diameter, and are uniformly covered by PDOT. XRD performed on P@CN/G sample clearly suggests the coexistence of both CoNi@C-BTC and graphene phases in the nanocomposite while XPS characterization confirms that Co, Ni, C, and O are detected in the P@CN/G sample. VSM measurements reveal S-like hysteresis loops for both CN, CN/G and P@CN/G, confirming soft magnetic materials and ferromagnetic behavior which linked to the presence of ferromagnetic Co and Ni nanoparticles in the nanocomposite powder. Electromagnetic parameters, namely dielectric permittivity, magnetic permeability and associated losses, are measured for P@CN/G composite sample dispersed into epoxy resin with 15%, 20%, 25% and 30% concentration using a vector network analyzer. Measured parameters are used to predict by simulations the return losses (RL) for various combinations of thickness and concentration. It is concluded from the exhaustive comparison using a FOM gauge that sample having 30% concentration and thickness 2.4 mm achieves the best performance, i.e. a value FOM equal to 1150 and minimal return losses RL equal to −50 dB.

1. Introduction

As stated in [1] the ever growing increase of communications systems induces a crucial need for lightweight devices combining compactness and reliability. The constraints are antagonist if we consider that reduced size increases the risk of harmful electromagnetic interferences between electronic components. The same risk occurs from the wireless propagation which may be detrimental to both electronic devices and human body [2]. Therefore, since more than one decade, research is conducted on efficient microwave absorbing structures (MAS) aiming at blocking such interferences. Among these, polymer composites combining conductive charges and polymer hosting matrix offer several advantages; high conductivity at low loading rate owing to very good dispersion, mechanical stiffness as well as possibility of conformability for stealth application, lightweight as compared to metallic shields, etc. MAS can be designed to reduce the radar cross-section (RCS) of various objects for military as well civil applications: an absorbing shield covering the target is used to reduce by absorption the signal reflected by the target towards the radar, making the target almost invisible to radar (concept of stealth). Well-known applications are military airplanes (stealth bombers) and towers of wind farms, that need to be stealth for security reasons, i.e., to ensure invisibility or avoid spurious signatures perturbing the control of the traffic in civil air traffic. A dedicated family of absorbers is developed to reduce the RCS: the Salisbury screen configuration [3,4], based on an absorbing layer covering the target assumed to be metallic, thus reflective. The conductivity of the layer and its thickness can be tuned in order to match the frequency and bandwidth of the absorption, depending on the applications. A well-known case is radar communications at X band (8–12.4 GHz) [5]. In [6,7], various MAS are studied, where carbon fillers, including carbon black, incorporated at different concentration levels in single as well as multilayer configurations, induce reflection below −10 dB. A good absorber aims at minimizing the reflection of a signal incident to its surface, while maximizing the absorption through its thickness. Conductive composites are suited to attenuate the signal, however conductive charges may also increase the reflection as do metallic shields. An adequate strategy in order to counterbalance this effect consists in incorporating magnetic charges into the composite [8–11]. This combination allows to decrease the equivalent impedance at input interface as close as possible to that of air. The reflection is consequently re-

* Corresponding author.
Email addresses: yancao162@gmail.com (Y. Cao); abdeliazim.mohamed.mustafa@gmail.com (A.M. Mohamed); mehdi.umbo@gmail.com (M. Abdollahzadeh); isabelle.huynen@uclouvain.be (I. Huynen)

https://doi.org/10.1016/j.jallcom.2020.158371
0925-8388/

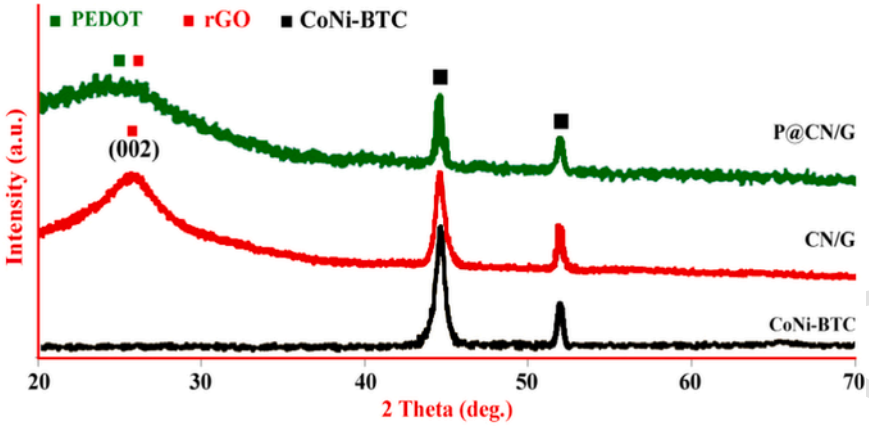

Fig. 1. The XRD patterns of a CoNiBTC, CN/G and P@CN/G samples.

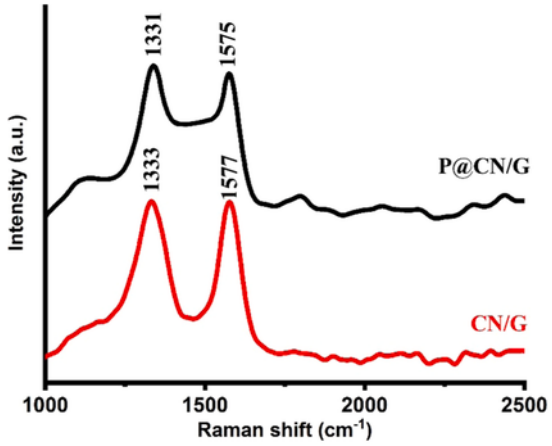

Fig. 2. Raman spectra of CN/G and P@CN/G samples.

duced and absorption favored via the penetration of the signal in the absorber. In the overall context of developing light-weight and thin broadband MAM absorber, majority of research is devoted to nanofiller surface modification, high concentration multi-filler nanocomposite, and automated numerical techniques to synthesis randomly arranged multilayer topologies of nanocomposite, so in [12–16].

In this paper we propose a microwave absorber based on composite materials containing CoNi@C-BTC (benzenetricarboxylic acid)/rGO nanocomposite (CN/G). Nanocomposite powders are prepared and dispersed into epoxy, and then simulated numerically, with the objective to decrease return loss associated to RCS and therefore increase the absorption through the samples. Section 2 details the synthesis procedure of CoNi@C-BTC/rGO nanocomposite (CN/G), as well as morphological and microwave characterization tools. Section 3 provides the structural/morphological analysis as well as the demonstration of the absorption performances of our composite through measurements of electromagnetic parameters and resulting minimal reflection losses observed in our structures. It also provides a comparison of performances between absorbers using novel figures of merit as gauges, while Section 4 concludes about our work.

2. Materials and test method

2.1. Preparation of CoNi@C-BTC/rGO Nanocomposite (CN/G)

Solvothermal process and pyrolysis treatment were utilized for synthesizing the CoNi@C-BTC (CN) and CoNi@C-BTC/rGO (CN/G) nanocomposites as follow:

Stoichiometric amount of cobalt(II) nitrate ($Co(NO_3)_2$) and nickel(II) nitrate $Ni(NO_3)_2$ were dissolved in dimethylformamide (DMF) and after preparation the stable solution, as-purchased functionalized GO (5 wt% of CoNi-BTC procedure weight) was added and ultrasonically dispersed for 1 h. Then another DMF based solution containing 1,3,5-trimesic acid (H_3BTC) and poly(N-vinyl-2-pyrrolidone) was prepared and added drop-wisely into the first solution and mixed vigorously for another 1 h. The final suspension was sealed in stainless steel Teflon lined autoclave at the temperature of 180 °C for 12 h. The centrifuged product was washed several times with deionized water/ethanol and dried in vacuum oven at 90 °C for 24 h. Finally, the dried product was pyrolyzed at 700 °C for 2 h under N_2 atmosphere.

2.2. Coating CN/G nanocomposite with PEDOT polymer (P@CN/G)

PEDOT was coated on nanocomposite via oxidative chemical polymerization of 3,4-ethylenedioxythiophene (EDOT) monomer. First, equal weight ratio of monomer: nanocomposite was added to the precooled (0–5 °C) 1 M solution of camphorsulfonic acid. Another 1 M camphorsulfonic acid solution containing an appropriate amount of ammonium peroxydisulfate (APS) was prepared and poured drop-wisely into the first suspension. The final mixture was continuously stirred for 2 h at 0–5 °C. The dark green precipitate was washed several times and dried in vacuum oven at 70 °C for 10 h.

2.3. Characterizations

Crystal structure and chemical state were characterized via X-ray diffraction (XRD, Bruker-AXS D8) and X-ray photoelectron spectroscopy (XPS) (VG ESCALAB250Xi electron spectrometer, Al K_α monochromator X-ray source), respectively. Raman spectra was provided via Raman spectrometer (WITec Alpha300R, 514 nm laser) for specific structural features of carbon base materials. Microstructure was evaluated by scanning electron microscopy (FESEM, TESCAN MIRA3 LMU). Magnetic properties were evaluated with vibrating sample magnetometer (VSM, Lakeshore, new 7307 series).

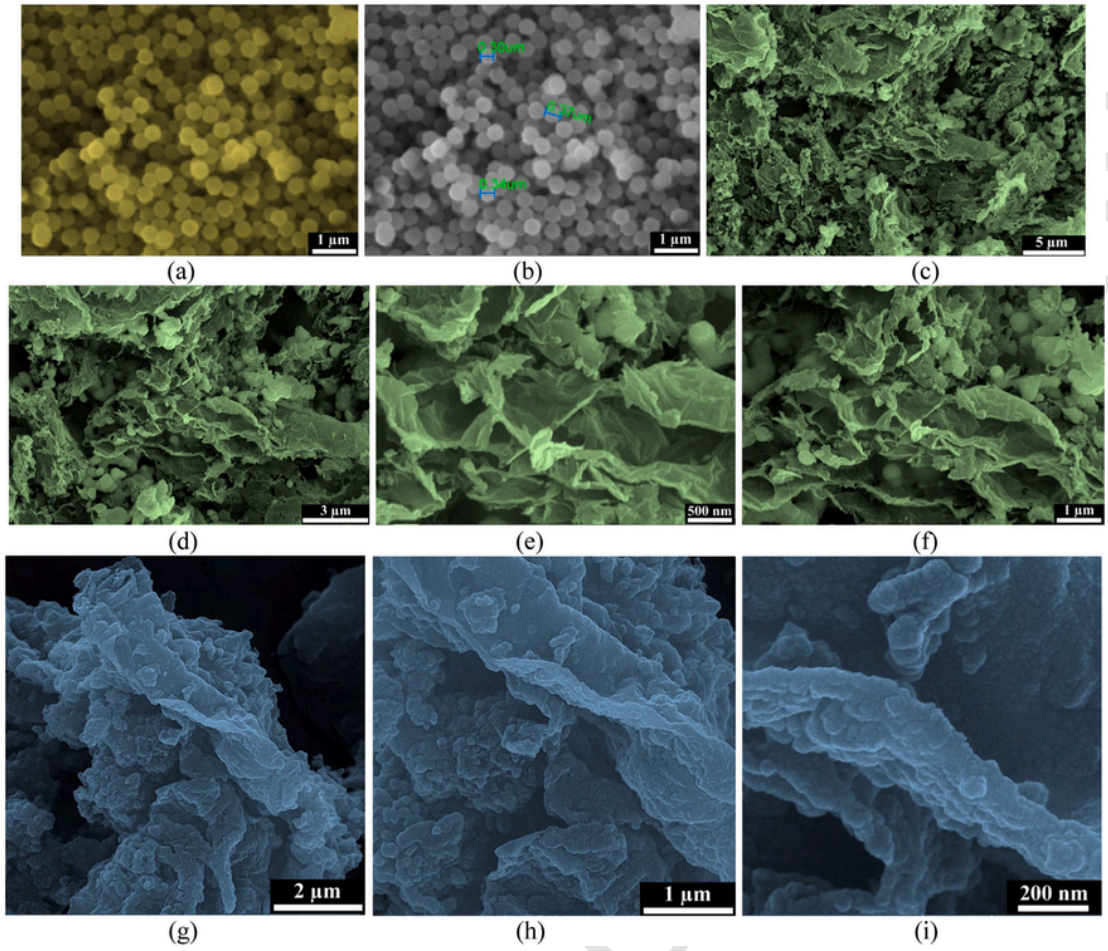

Fig. 3. FESEM images of, a and b) CoNi-BTC, c–f) CN/G and g–i) P@CN/G.

2.4. Electromagnetic measurements

In order to evaluate the electromagnetic wave absorption characteristics of single layer samples in X-band frequency, 15, 20, 25 and 30 wt% of the P@CN/G powder was dispersed in resin epoxy matrix and molded with 2, 2.4, and 2.8 mm thickness. The relative complex permittivity and complex permeability were measured by using a vector network analyzer (Agilent N5230A).

3. Results and discussion

3.1. Physico-chemical characterization

3.1.1. Structural characterization

The structural characterization and phase constituents of the nanocomposites was carried out using X-ray powder diffractometer (XRD). Fig. 1 demonstrates the XRD patterns of as-prepared CoNi@C-BTC, CN/G and P@CN/G samples. As it can be seen in CoNi-BTC pattern, 2 sharp diffraction peaks at 44.4° and 51.7° corresponding to (111) and (200) of FCC (face-centered cubic) structure of CoNi alloy which coincides with both pure Co and Ni phases with 15-0806 and 04-0850 JCPDS card numbers, respectively. Within this resolution, there is no distinguishable peak related to carbon due to low-temperature of pyrolysis process. CN/G curve clearly suggests the coexistence of both CoNi@C-BTC and graphene phases in the nanocomposite. The detected diffraction peak at 26°, which representing the characteristic plane of (002) of graphitic carbon, indicated the reduction of GO to rGO during the solvothermal method. It could be seen in P@CN/G curve, broad peak lying between 20° and 26° confirms the overlapping of both amorphous polymer and rGO phases in the nanocomposite. No conspicuous difference can be observed after coating particles with polymer just reduction in the peaks intensity of CoNi@C-BTC phase.

Fig. 2 illustrates the Raman spectra of as-prepared CN/G and P@CN/G samples. The D bands peak located at ~1333 cm^{-1} and G bands peak located at ~1577 cm^{-1} represent vibration of aromatic rings and sp^2-bonded of carbon, respectively. Furthermore, the intensity ratio between D and G bands (I_D/I_G) ascribed to the extent of disorder or degree of graphitization. The I_D/I_G values for CN/G and P@CN/G samples are 1 and 1.02. The slight increment of I_D/I_G value in P@CN/G sample stems from the π conjugated structure and also ring stretching mode of PEDOT polymer. The charge redistribution between multiple interfaces causes slight blue shift of D and G bands for the P@CN/G sample which suggests the anchoring between polymer, rGO and CoNi-BTC powders.

3.1.2. Morphological characterization

Fig. 3(a and b) shows the morphology of CoNi-BTC sample. As it can be seen, approximately uniform monodispersed nanospheres (mean particle size ~300–400 nm) were formed. According to Fig. 3(c–f) intimate coexistence of both CoNi-BTC and graphene sheets

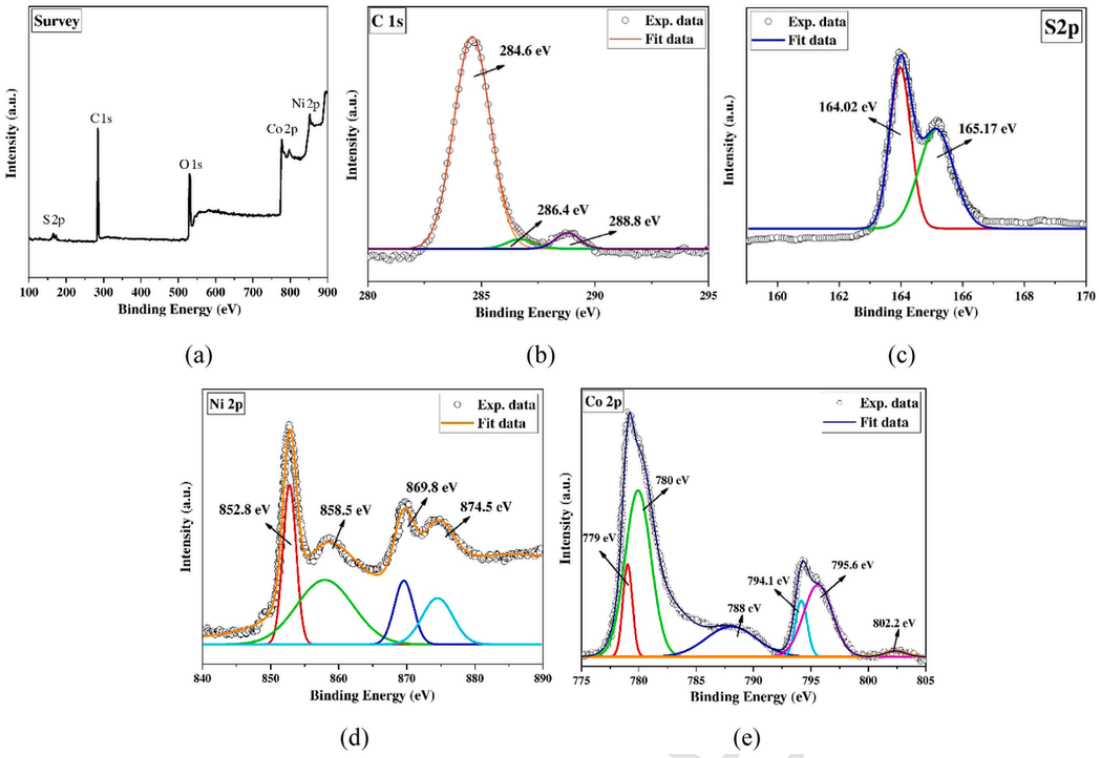

Fig. 4. XPS spectra of the P@CN/G, a) survey scan b) C 1s spectrum, c) S 2p spectrum, d) Ni 2p spectrum and e) Co 2p spectrum of this sample.

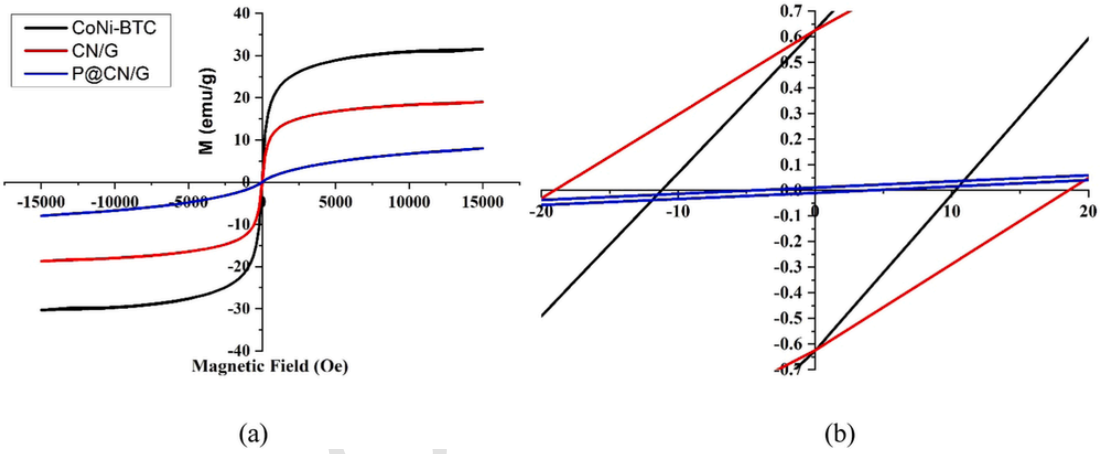

Fig. 5. a) Room temperature magnetic hysteresis loops of as-prepared samples, b) corresponding enlarged view.

Table 1
Magnetic parameters of as-prepared samples.

	Ms (emu/g)	Mr (emu/g)	Hc (Oe)
CoNi-BTC	31.60	0.62	11.20
CN/G	19.07	0.61	18.85
P@CN/G	7.95	0.01	4.42

are revealed. From the FESEM images (Fig. 3(g–i)) we can evidently observe small bumps on the surface of the particles and graphene sheets which confirms uniformly coating of PEDOT on the surface due to strong intermolecular force between EDOT and surface organic groups of CoNi-BTC and graphene sheets. To sum-up, images confirmed the prosperous formation of PEDOT polymer on the nanocomposite without any damage to the original shape of the components.

3.1.3. XPS characterization

The elemental status of P@CN/G sample was evaluated by X-ray photoelectron spectroscopy (XPS). Based on the full survey spectrum (Fig. 4a), Co, Ni, C, and O are detected in this sample. As shown in Fig. 4(b), the deconvolution spectra of C1s exhibits three peaks at 284.6, 286.4 and 288.8 eV which correspond to C-C, C-O and C ═O functional groups. Moreover, the co-existence of C1s and S2p (164.02 and 165.17 eV) peaks confirm the formation of PEDOT (Fig. 4(c)). The high resolution Ni 2p spectra can be deconvoluted by four

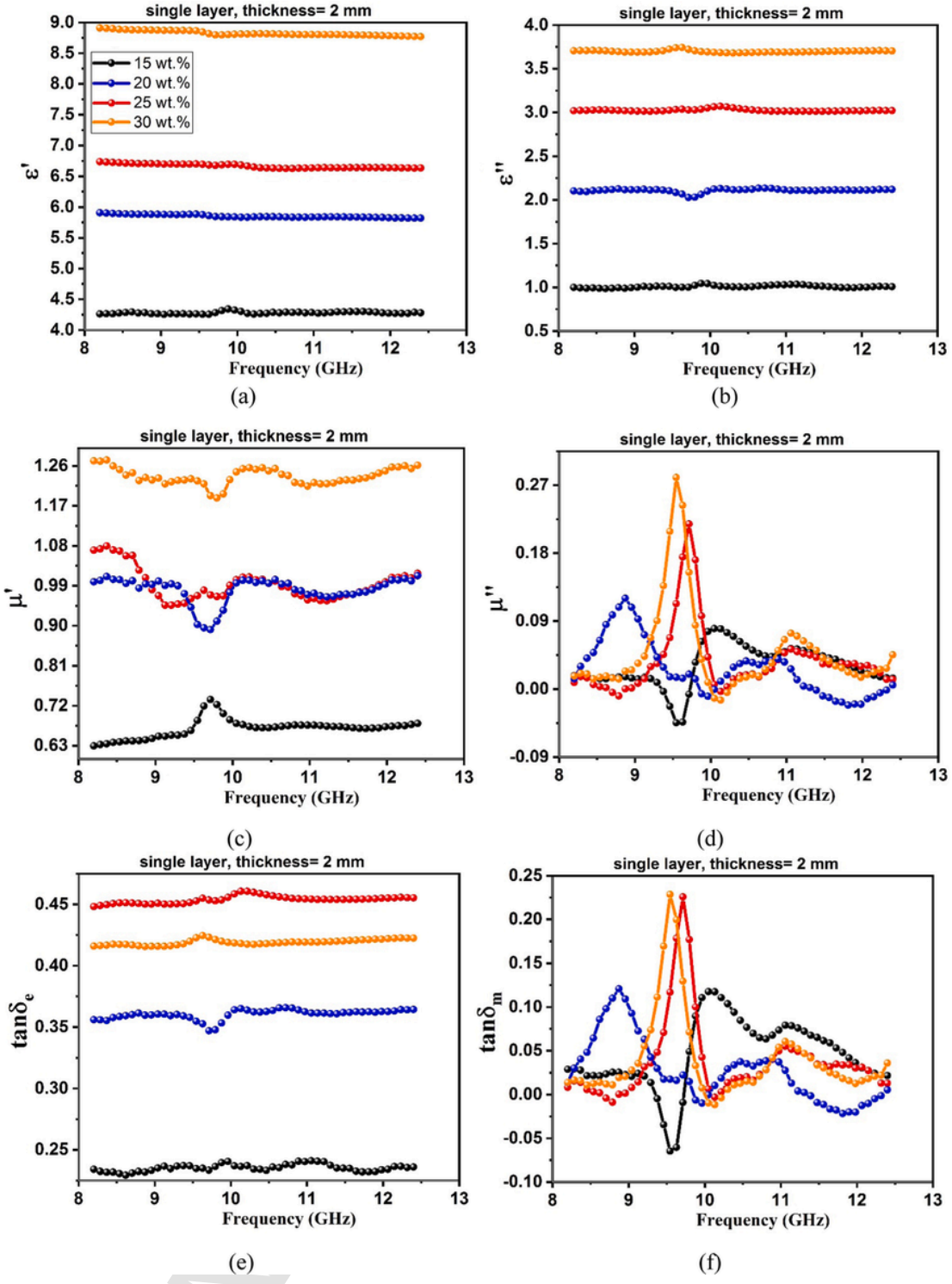

Fig. 6. Electromagnetic parameters: complex permittivity (a,b), complex permeability (c,d), tan δ_ε (e), and tan δ_μ (f) of P@CN/G sample composites in 8–12 GHz frequency range.

characteristic peaks at 852.8 and 869.8 eV related to the Ni $2p_{3/2}$ and Ni $2p_{1/2}$ of metallic Ni respectively. Furthermore, characteristic peaks at 858.5 and 874.5 eV binding energies can be attributed to the Ni $2p_{3/2}$ and Ni $2p_{1/2}$ of Ni^{2+} states and also satellites peaks were detected at 858.5 and 874.5 eV (Fig. 4(d)). The Co 2p spectra (Fig. 4e), is decomposed into 4 main peaks at 780 and 795.6 eV (belong to Co $2p_{3/2}$ and Co $2p_{1/2}$ electrons) and also 779 and 794.1 eV (signals of metallic Co state). Moreover, two shake-up satellites peaks at 788.9 and 802.2 eV binding energies.

3.2. Magnetic properties

The room temperature magnetic behavior of as-prepared samples was evaluated via VSM with an external magnetic field of 1.5 T (Fig.

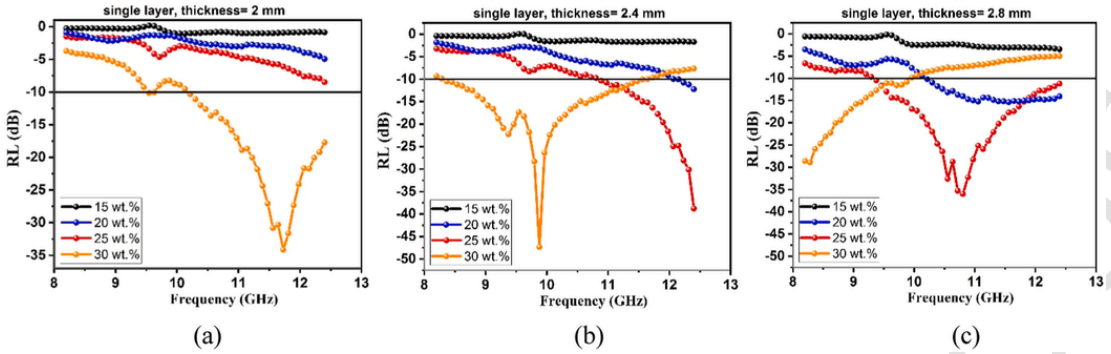

Fig. 7. Calculated RL curves of P@CN/G sample with, a) 2 mm thickness, b) 2.4 mm thickness and c) 2.8 mm thickness.

Table 2
Comparison of performances for samples satisfying RL < −10 dB.

Sample	thickness (mm)	Fo (GHz)	BW (GHz)	|RL= (dB)	FB (%)	FOM	d_N	FOM_N
25%	2.4	12.5	2	40	16	640	1	640
25%	2.8	10.8	3	35	28	980	1.008	972
30%	2	11.6	2.8	35	17	595	0.813	732
30%	**2.4**	**9.8**	**3**	**50**	**23**	**1150**	**0.7843**	**1466**
30%	**2.8**	**8**	**3**	**30**	**37**	**1110**	**0.7467**	**1486**

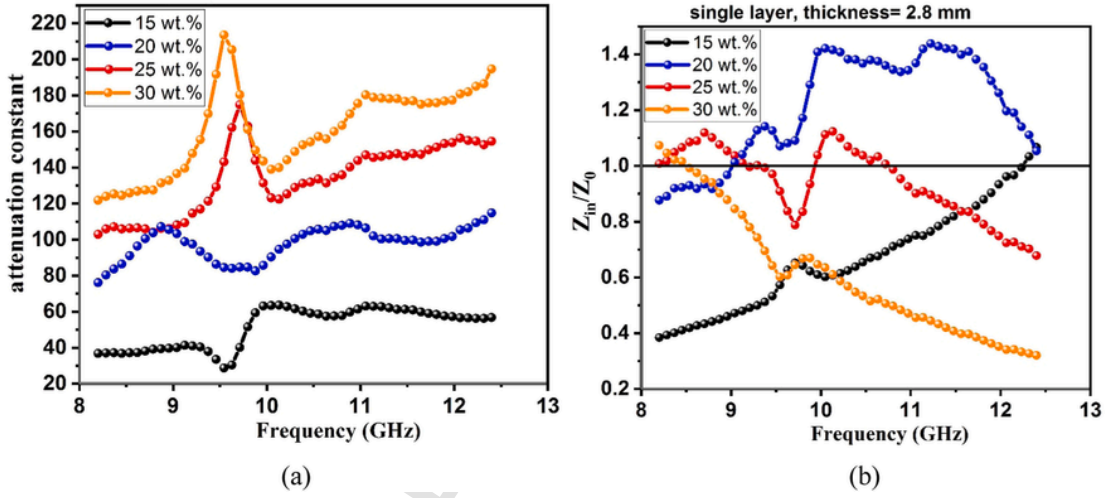

Fig. 8. (a) Attenuation coefficient α (b) ratio |Zin/Z0|.

5). The magnetic parameters (saturation magnetization (M_s), remanent magnetization (M_r) and coercivity field (H_c)) are summarized in Table 1. According to the results, symmetric closed hysteresis loops are observed for all samples while coercivity lower than 20 Oe proves typical soft ferromagnetic behavior. The magnetization (M_s) value of CoNi-BTC sample is much higher than both CN/G and P@CN/G samples. The decrement of the saturation magnetization value occurs by introduction of graphene and PEDOT polymer as non-magnetic phases in the nanocomposite.

3.3. Electromagnetic properties

3.3.1. Electromagnetic parameters

The electromagnetic parameters were obtained from the sample prepared as described in Section 2.4 that also explains the measurement and extraction technique.

The behavior as a function of the concentration shown in Fig. 6 is as expected. The dielectric losses (Fig. 6(b)) are induced by the presence of PEDOT covering CN/G particles as well as graphene, these two constituents being conductive and inducing dielectric losses by virtue of the relation: $\tan\delta = \sigma/(2\pi f\,\varepsilon'\,\varepsilon o)$. The conductive PEDOT coating improved the interfacial polarization due to bound and bipolaron/polaron charges that resulted in higher permittivity values [17]. As the content of P@CN/G increases in the epoxy, so does the conductivity, hence the dielectric losses. The increase of dielectric constant with concentration (Fig. 6(a)) is ascribed to the Maxwell-Wagner-Sillars effect well known and observed in dielectric materials loaded with conductive charges [18,19].

The same reasoning holds for magnetic permeability and magnetic losses. Both increase with concentration in P@CN/G particles due to the magnetic content ascribed to the presence of Co and Ni particles in the powder. The values however are rather low since magnetic parameters shown in Table 1 have lowest values for P@CN/G particles.

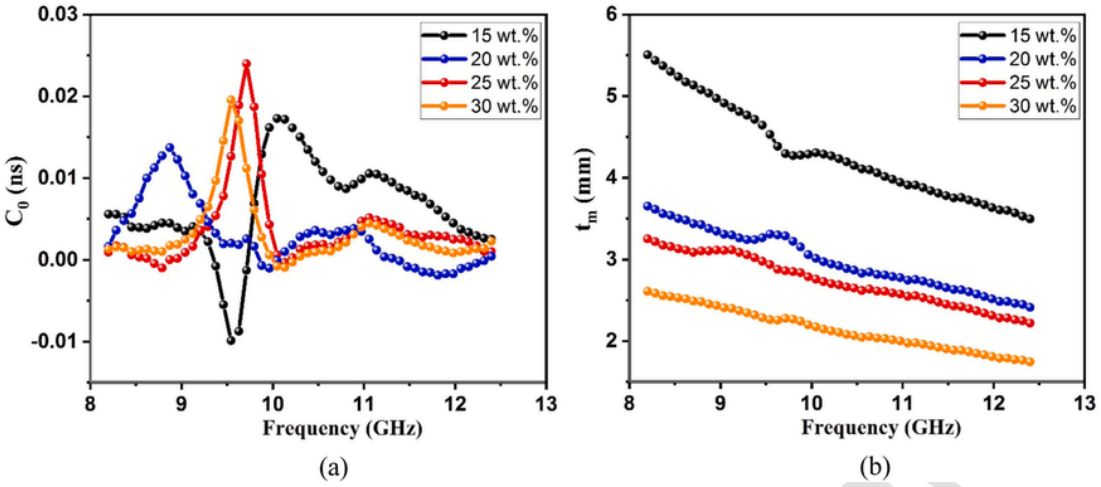

Fig. 9. (a) C_0 curves (b) t_m curves of P@CN/G sample.

3.3.2. Microwave absorption capability

As done in [1] the microwave absorption capability of our samples was studied via the evaluation of return losses (*RL*) associated to reflection of samples in a Salisbury screen configuration, that is when the absorbing sample is backed by a metallic plate. This configuration mimics the radar operation where signal incident to a target is reflected, allowing its detection by the radar. For stealth applications, *RL* has to be minimized in order to make the target invisible. The Salisbury configuration is adequate to evaluate the absorption capability of a material through the measurement of *RL* since if *RL* is minimized, it means that all signal has been absorbed in the sample so that almost nothing is reflected (nor transmitted since the metallic plate blocks the propagation). *RL* in Salisbury configuration expresses as the reflection coefficient at input interface of an absorber and depends on the input impedance Z_{in} [20]:

$$RL = 20 \quad \log_{10}\left(\frac{Z_{in} - Z_O}{Z_{in} + \quad Z_O}\right) \tag{1}$$

$$Z_{in} = \sqrt{\frac{\mu}{\varepsilon}} Z_o \tanh(\gamma d) \tag{2}$$

where

$$\gamma = \quad j \quad 2 \quad \pi f \sqrt{\varepsilon \left(\quad 1 - j \quad \tan\delta_\varepsilon \right) \mu \quad \left(1 - j \tan\delta_\mu\right)} / c_O \tag{3}$$

Z_o is the free-space impedance equal to 377 Ohms, f is the frequency, d is the thickness of the sample and ε, μ, $\tan\delta_\varepsilon$, $\tan\delta_\mu$ are measured permittivity, permeability and associated loss tangent factors given in Fig. 6, respectively, while c_o is the light velocity in air. The electromagnetic parameters of the sample have thus an impact on *RL*.

From Eq. (1) it can be derived that *RL* is minimum, hence the absorption is maximum, when the imaginary part of Z_{in} cancels: this occurs when the thickness d of the sample is a multiple of a quarter wavelength λ/4, i.e. at specific frequencies f_e

$$\begin{aligned} d &= n\frac{\lambda}{4} \\ &= nC_O / \left(4 \quad f\sqrt{\varepsilon\mu}\right) \\ &\rightarrow \quad f_O \\ &= nc_o / \left(d \quad 4 \quad \sqrt{\varepsilon\mu}\right) \end{aligned} \tag{4}$$

Fig. 7 compares the *RL* values versus frequency at X band for various concentrations and thicknesses d of the samples. Only samples having concentrations 25% and 30% succeed to meet the $RL < -10$ dB criterion qualifying a good absorber, while those having concentrations 15% and 20% fail over almost the whole frequency range.

Table 2 compares the performances for concentrations 25% and 30%, and thickness $d = 2$, 2.4, and 2.8 mm.

In view of this the following definitions are proposed:

- the −10 dB bandwidth, noted BW and defined as the frequency range where RL < −10 dB
- the fractional bandwidth defined as FB = BW/f_o, where f_o is the center frequency of the absorption bandwidth BW
- The figure of merit (FOM) is a quantity used to characterize the performance of a device, system or method, relative to its alternatives. In engineering, figures of merit are often defined for particular materials or devices in order to determine their relative utility for an application. In our case, the microwave absorber, the figure of merit is defined as FOM = FB x |RL = ; this figure indicates that we are interested in having the highest magnitude of reflection losses |RL = over the highest possible frequency range.
- The normalized thickness d_N, defined as the thickness expressed as fraction of the wavelength λ_o at frequency f_o.
- The normalized FOM noted FOM_N, defined as $FOM_N = FOM/d_N$, which aims at gauging the compacity of the absorber; the lower the thickness and the higher the FOM, so the highest is the FOM_N.

From Table 2 it can be concluded that 2 samples, marked in bold face, stand out in term of FOM. They have a respective thickness equal to 2.4 and 2.8 mm. Their superiority results from the fact that both FB and | RL = are higher than for most of the other samples. When thickness is taken into account through FOM_N, the sample having thickness $d = 2.8$ mm shows the best performance. The two sam-

ples also have the highest concentration of 30%, which allows to minimize the reflection loss *RL* responsible for absorption in the material.

The absorber operating in Salisbury configuration exploits a resonant behavior occurring when the thickness *d* of the sample is a multiple of the operating wavelength according to Eq. (4); at the corresponding frequency the reflected signal returns to the input of the absorber with a 180° phase shift while being almost totally attenuated by absorption induced by the lossy material characterized by the attenuation constant $\alpha = Re\ (\gamma)$ from (3) shown in Fig. 8(a), so that Z_{in} becomes a real number proportional to the losses in the material. As expected it increases with the wt% concentration, as following dielectric and magnetic losses shown in Fig. 6(e,f). The higher the losses in the material, the more Z_{in} is close to Z_o, minimizing thus *RL* by virtue of Eq. (1). This is demonstrated in Fig. 8(b) that illustrates the behavior of the magnitude of Z_{in} / Z_o as a function of frequency and concentration for the sample with thickness d = 2.8 mm. Only the 25% concentration allows the Z_{in} impedance to reach the Z_o impedance over a significant frequency range, namely from 9 GHz to 12 GHz, explaining the low *RL* values in this frequency range observed in Fig. 7(c). Concentration 30% should achieve even better performance but this is not visible in the figure since resonance reasonably occurs below 8 GHz, owing to higher values of permittivity and by virtue of Eq. (4).

The eddy current loss coefficient C_0 and microwave attenuation constant α are expressed by the following equations:

$$C_0 = \mu'' \mu'^{-2} f^{-1} = 2\pi \mu_0 \sigma d^2 \tag{5}$$

$$\alpha = \frac{2\pi}{c}\sqrt{2\mu'\varepsilon'}\sqrt{\frac{\mu''\varepsilon''}{\mu'\varepsilon'} - 1 + \sqrt{\left(\frac{\mu''}{\mu'}\right)^2 + \left(\frac{\varepsilon''}{\varepsilon'}\right)^2 + \left(\frac{\mu''\varepsilon''}{\mu'\varepsilon'}\right)^2 + 1}}$$

where d, μ_0, and σ represent thickness, permeability in vacuum and electrical conductivity, respectively. As expected from Eq. (6), which shows that α is proportional to ε" and μ", the attenuation constant is higher for 30% concentration, this is owing to the respective values shown in Fig. 6(c,d). As known to all, if the magnetic loss is caused by the eddy current loss mechanism, then C_0 values should be constant by increasing the frequency [15]. This is indeed verified in Fig. 9(a). Fig. 9(b) shows the matching thickness t_m as a function of frequency, for each concentration: it can be obtained from inverting Eq. (4) in order to obtain the thickness *d* where *RL* is minimum, inducing matching. Obviously t_m decreases with frequency and with increased concentration since the latter increases to both dielectric constant and permeability, as shown in Fig. 6(a and c).

4. Conclusion

In this paper CoNi-BTC (CN) mixed with reduced graphene oxide and covered by PDOT to form P@CN/G were successfully synthesized via solvothermal method followed by pyrolysis and characterized with XRD, XPS, VSM and FESEM.

XRD performed on P@CN/G sample clearly suggests the coexistence of both CoNi@C-BTC and graphene phases in the nanocomposite while XPS characterization confirms that Co, Ni, C, and O are detected in the P@CN/G sample.

FSEM images show that CoNi-BTC particles have an approximately uniform spheroidal monodispersed morphology with 300–400 nm diameter, and are covered uniformly covered by PDOT.

VSM measurements reveal S-like hysteresis loops for both CN, CN/G and P@CN/G, confirming soft magnetic materials and ferromagnetic behavior which linked to the presence of ferromagnetic Co and Ni nanoparticles in the nanocomposite powder.

Electromagnetic parameters, namely dielectric permittivity, magnetic permeability and associated losses, are measured for P@CN/G composite sample dispersed into epoxy resin with 15%, 20%, 25% and 30% concentration. Measured parameters are used to predict by simulations the return losses (RL) for various combinations of thickness and concentration. It is concluded from the exhaustive comparison using a FOM gauge that sample having 30% concentration and thickness 2.8 mm achieves the best normalized FOM value superior to 1100 while sample with thickness 2.4 mm achieves minimal return losses RL equal to −50 dB.

Conflict of interest

The author declares no conflict of interest.

Declaration of Competing Interest

The authors declare that they have no known competing financial interests or personal relationships that could have appeared to influence the work reported in this paper.

References

[1] Rozhin Sadeghi, Abbas Sharifi, Marta Orlowska, Isabelle Huynen, Investigation of microwave absorption performance of CoFe2O4/NiFe2O4/Carbon fiber composite coated with polypyrrole in X-band frequency, Micromachines 11 (2020) 1–13article 809 (August).

[2] N. Violette, Electromagnetic Compatibility Handbook, Springer, Berlin/Heidelberg, Germany, 2013.

[3] B. Chambers, Optimum design of a Salisbury Screen radar absorber, IEEE Electron. Lett. 30 (1994) 1353–1354.

[4] J.B. Kim, Design of Salisbury screen absorbers using dielectric lossy sheets, in: Proceedings of the 2011 IEEE International Conference on Microwave Technology & Computational Electromagnetics, Beijing, China, 22–25 May 2011, pp. 1–2.

[5] J.-H. Oh, K.-S. Oh, C.-G. Kim, C.-S. Hong, Design of radar absorbing structures using glass/epoxy composite containing carbon black in X-band frequency ranges, Compos. Part B 35 (2004) 49–56.

[6] J.-B. Kim, S.-W. Lee, C.-G. Kim, Comparison study on the effect of carbon nano materials for single-layer microwave absorbers in X-band, Compos. Sci. Technol. 68 (2008) 2909–2916.

[7] B. Kim Adv. Compos. Mater. 21 (2012) 333 Publisher:City, Country

[8] P.M. Raj, D. Mishra, H. Sharma, S. Swaminathan, R. Tummala, Nanomagnetic materials and structures, and their applications in integrated rf and power modules, Nanomagnetism (2014) 1–29.

[9] F. Qin, H.X. Peng, N.Y. Pankratov, M. Phan, L.V. Panina, M. Ipatov, V. Zhukova, A. Zhukov, J. Gonzalez, Exceptional electromagnetic interference shielding properties of ferromagneticmicrowires enabled polymer composites, J. Appl. Phys. 108 (2010), 044510.

[10] X. Ma, Q. Zhang, Z. Luo, X. Lin, G. Wu, A novel structure of ferroaluminum-based sandwich composite for magnetic and electromagnetic interference shielding, Mater. Des. 89 (2016) 71–77.

[11] K. Singh, A. Ohlan, A. Bakhshi, S. Dhawan, Synthesis of conducting ferromagnetic nanocomposite with improved microwave absorption properties, Mater. Chem. Phys. 119 (2010) 201–207.

[12] D. Micheli, R. Pastore, A. Vricella, M. Marchetti, Matter's electromagnetic signature reproduction by graded-dielectric multilayer assembly, IEEE Microw. Theory Tech. 65 (8) (2017) 2801–2809.

[13] Shital Patangrao Pawar, High frequency millimetre wave absorbers derived from polymeric nanocomposites, Polymer Vol 84 (2016) 398–419.

[14] Jean-Michel Thomassin, Polymer/carbon based composites as electromagnetic interference (EMI) shielding materials, Mater. Sci. Eng. R Rep. 74 (7) (2013) 211–232.

[15] Fusheng Wen, Fang Zhang, Zhongyuan Liu, Investigation on microwave absorption properties for multiwalled carbon nanotubes/Fe/Co/Ni nanopowders as lightweight absorbers, J. Phys. Chem. C 115 (29) (2011) 14025–14030.

[16] Zhou Wang, Guang-Lin Zhao, Electromagnetic wave absorption of multi-walled carbon nanotube–epoxy composites in the R band, J. Mater. Chem. C 2 (2014) 9406–9411.
[17] X. Ni, X. Hu, S. Zhou, C. Sun, X. Bai, P. Chen, Synthesis and microwave absorbing properties of poly(3,4-ethylenedioxythiophene) (PEDOT) microspheres, Polym. Adv. Technol. 22 (2011) 532–537.
[18] A. Emplit, I. Huynen, Study of absorption in carbon nanotube composites from 1HZ to 40GHZ, (January) Int. J. Microw. Eng. 2 (1) (2017) 01–13(January).
[19] A. Saib, L. Bednarz, R. Daussin, C. Bailly, X. Lou, J.-M. Thomassin, C. Pagnoulle, C. Detrembleur, R. Jerome, I. Huynen, Carbon nanotube composites for broadband microwave absorbing materials, IEEE Trans. Microw. Theory Tech., vol 54 (6) (2006) 2745–2754(June) (EuMC2005 Spec. Issue).
[20] D. Pozar, Microwave Engineering 2nd edition, Wiley, New York, NY, USA, 1998.